UC Berkeley

Building Efficiency and Sustainability in the Tropics (SinBerBEST)

Title
Polymer lattice-reinforcement for enhancing ductility of concrete

Permalink
https://escholarship.org/uc/item/3781m1pg

Authors
Salazar, Brian
Aghdasi, Parham
Williams, Ian D
et al.

Publication Date
2020-09-28

Peer reviewed

1 **Polymer lattice-reinforcement for enhancing ductility of concrete**

2 Brian Salazar[a1], Parham Aghdasi[b], Ian D. Williams[b], Claudia P. Ostertag[b], Hayden K. Taylor[a1]

3 [a] Department of Mechanical Engineering, University of California, Berkeley, Berkeley, CA,

4 USA

5 [b] Department of Civil and Environmental Engineering, University of California, Berkeley,

6 Berkeley, CA, USA

9 **Highlights**

10 • Ultra-high-performance concrete was reinforced with 3D-printed, stretch-dominated

11 polymeric lattices, resulting in greatly increased ductility

12 • Ductility was optimized by deliberately orienting 3D printed polymer filaments in line with

13 the expected tensile stresses.

14 • The ductility-enhancing mechanisms during flexure are associated with multiple cracking

15 and tortuous crack paths.

16 • This fabrication method allows easy pouring of the mortar mixture, unlike polymer fiber-

17 reinforced composites.

[1] Corresponding authors. Email addresses: brian10salazar@berkeley.edu (B. Salazar); hkt@berkeley.edu (H. Taylor)

18　• This composite production method lends itself more readily to automated manufacturing than

19　　conventional steel rebar-reinforced concrete.

20　**Graphical abstract**

21　
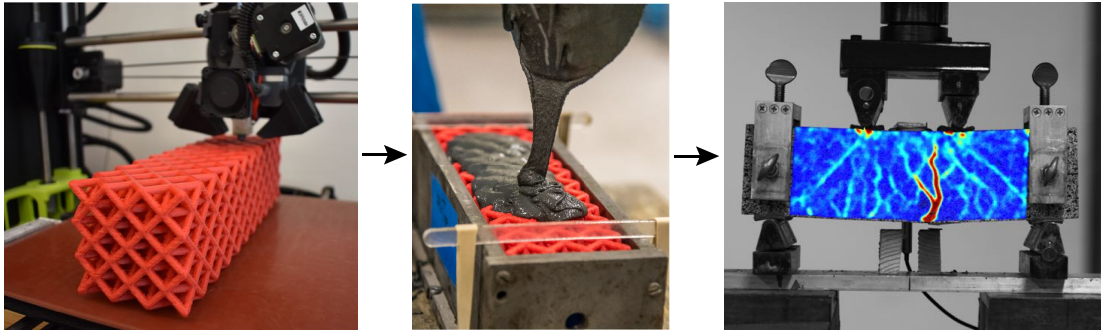
22　**Abstract**

23　Concrete is the most widely used engineering material. While strong in compression, concrete is

24　weak in tension and exhibits low ductility due to its low crack growth resistance. With increasing

25　compressive strength, concrete becomes even more brittle, hence requiring appropriate

26　reinforcement to enhance its ductility. This paper presents a new method for increasing the

27　ductility of ultra-high-performance concrete by reinforcing it with 3D printed polymeric lattices

28　made of either polylactic acid (PLA) or acrylonitrile butadiene styrene (ABS). These lattice-

29　reinforced concrete specimens were then tested in compression and four-point bending. The

30　effect of polymeric reinforcement ratios on mechanical properties was investigated by testing

31　two lattice configurations. The lattices were very successful in transforming the brittle ultra-

32　high-performance concrete (UHPC) into a ductile material with strain hardening behavior; all

33　flexural specimens revealed multiple cracking and strain hardening behavior up to peak load.

34　Increasing the ABS reinforcing ratio from 19.2% to 33.7% resulted in a 22% reduction in

35　average compressive strength. However, in flexure, increasing the PLA reinforcing ratio from

36　19.2% to 33.7% resulted in a 38% increase in average peak load. The compression results of all

37   specimens independent of their reinforcement ratio revealed smooth softening behavior in

38   compression.

1. Introduction

40   Concrete strikes a balance between performance, cost, and availability. It has enabled many of

41   the largest and most demanding engineering projects in the world, and also finds its place in less

42   grandiose projects such as home foundations and sidewalks. On its own, the brittle tensile

43   response and quasi-brittle compressive response of concrete would limit its usefulness to simple,

44   compression-only load cases. As such, it relies on the composite behavior provided by the

45   reinforcement to provide ductile, predictable response under many types of loading demands.

46   Steel rebar cages are traditionally used to provide the requisite reinforcement and can be

47   detailed to effectively resist certain load cases — but they also come with limitations. As

48   structural elements trend toward more slender beams and columns using higher strength

49   concrete, conventional reinforcement detailing may not be enough to resist large demands such

50   as seismic or blast loading. Furthermore, rebar cages with high reinforcing bar ratios are not only

51   very labor-intensive to construct but also difficult to infiltrate with concrete.

52   An alternative way to enhance the ductility of concrete is through the use of discrete steel

53   or polymer fibers. However, the fiber distribution in fiber-reinforced concrete composites cannot

54   be easily controlled, hence leaving sections for the cracks to propagate uninhibited [1–6]. This

55   heterogeneity leads to unpredictability in the overall performance of fiber reinforced composites

56   and can reduce the expected tensile strength and fracture toughness of the material [7]. The

57   continuity and predictability inherent to three-dimensional reinforcements could potentially be

58   the key to mitigating these issues.

59   Textile reinforced concrete (TRC) uses a similar principle, but in two dimensions, and

60   has been shown to provide excellent reinforcement. Being reinforced in only two dimensions,

61   however, TRCs have limited usefulness in structural applications, and are mainly used in repair

62   and in lightweight sandwich panels [8–15].

63   This paper investigates a new class of composites that utilizes three-dimensional lattice

64   structures as reinforcements to enhance the ductility of concrete. Here, we employ the octet-truss

65   geometry because it is known for its high specific stiffness and fracture toughness [16,17]. The

66   octet lattices were prototyped in acrylonitrile butadiene styrene (ABS) and/or polylactic acid

67   (PLA) using Fused Deposition Modeling (FDM) 3D printers. The use of a polymeric

68   reinforcement material — instead of a steel reinforcement — enables the polymer-reinforced

69   structures to be more lightweight, corrosion-resistant, and thermally insulating.

70   Previous research has used 3D printed polymers to reinforce cementitious material. The

71   present authors [18] provided the first investigation of three-dimensional octet lattice-reinforced

72   cementitious materials and found increased ductility while using a highly workable mortar.

73   Farina et al. reinforced cement mortar with polymeric 'fibers' — in the form of simple, discrete

74   7.5 mm-diameter cylindrical bars — that were 3D printed from a photopolymer resin [19]. They

75   found that augmenting the surfaces of the printed reinforcement cylinders with mm-scale

76   protrusions led to much greater strain hardening of the composite than did smooth reinforcement

77   rods of the same diameter and material. Samples with roughened reinforcement showed shear

78   failure under three-point bend tests, whereas structures reinforced with smoother cylinders

79   exhibited flexural failure. Nam et al., meanwhile, investigated the effects of reinforcement

80   orientation and distribution by 3D printing reinforcement networks of connected photopolymer

81   resin fibers with varying spatial distributions. They found some evidence of higher peak bending

82 strength when using a triangulated reinforcement structure whose mesh was denser in regions of

83 higher tensile stress [20]. However, the inherent brittleness of the cement was not significantly

84 mitigated in any of the specimens, possibly because of the relatively low volume fraction of

85 polymer reinforcement used.

86   Recently, Rosewitz et al. developed bio-inspired cement–polymer composites, and

87 evaluated a variety of cellular polymeric reinforcement structures which showed increased

88 ductility and, in some cases, higher peak strength than unreinforced mortar [21]. Xu et al. [22]

89 tested the performance of thin panels reinforced with honeycomb lattices manufactured in ABS

90 using FDM. Their panels demonstrated ductility and multiple cracking when tested in flexure.

91 Both Rosewitz's and Xu's work, however, used prismatic or "two-dimensional" reinforcement

92 geometries, which may limit their applicability to complex geometries or loading states.

93   Previous work, then, has shown the great potential of polymeric reinforcement, but

94 highlighted several areas where further work was needed before widespread adoption. Firstly, a

95 systematic means of incorporating fully 3D — as opposed to prismatic or 2D — reinforcement is

96 needed, to accommodate potentially complex cast geometries and loading requirements.

97 Secondly, the specific polymeric materials and printing method need to offer a plausible route

98 towards scaling up the process. To this end, extrusion of thermoplastic polymers offers a more

99 realistic prospect of large-scale production than the use of photopolymers, which tend to be

100 much more expensive than commodity thermoplastics per unit mass. Moreover, thermoplastic

101 extrusion can be scaled up by increasing nozzle diameter and using robotic printers, whereas

102 photopolymer deposition rates and printing volumes remain more limited, in spite of recent

103 progress.

104   The study presented here expands significantly upon our original demonstration of

105   polymeric lattice reinforcement [18] by providing more comprehensive data on the effect of

106   three-dimensional octet lattices on the mechanical performance of concrete. Crucially, whereas

107   the previous study used a conventional mortar, this study concentrates on reinforcement of an

108   ultra-high-performance-concrete (UHPC) which has previously been developed by some of the

109   present authors [23–26]. Polymer lattice reinforcement of UHPC would be particularly

110   advantageous: because of the advanced mortar's higher cost of production, optimized

111   reinforcement geometries that can limit the amount of mortar used in a particular application

112   would significantly expand its potential uses. Moreover, one of the objectives of UHPC in the

113   first place is to reduce the amount of cement and associated CO_2 emissions required for a given

114   load, and using a reinforcement strategy in which a significant volume fraction is *non-*

115   *cementitious* can compound this advantage. Such a strategy is shown in this work, with

116   polymeric volume fractions exceeding 30% in some cases. The polymeric phase could in

117   principle be made from recycled material, cutting the carbon footprint further.

118   UHPC is, however, far more brittle than normal concrete, and hence may be expected to

119   interact mechanically with the reinforcement in different ways and to be more difficult to

120   enhance in ductility. It is therefore important to study whether the same degree of ductility

121   enhancement can be achieved in UHPC as in conventional mortar, and with what degree, if any,

122   of peak strength loss.

123   In this paper, we show how UHPC's ductility can be successfully increased with 3D

124   reinforcement lattices printed from PLA or ABS, which are widely used in additive

125   manufacturing and are available at reasonable cost. ABS is certainly already used for concrete

126   reinforcement — for example, the carbon fiber-reinforced ABS in the "C-Fab" process marketed

6

127 by Branch Technology [27]. For very high production volumes and rates, lattices could

128 potentially be manufactured using other processes, including modified molding or casting

129 processes. Additionally, while in this work we explore geometrically regular 3D lattices, there is

130 the potential to spatially vary the lattice parameters — such as the polymer volume fraction — to

131 accommodate complex loading conditions. It may even be possible to localize reinforcement

132 material in regions where tensile loads are predicted, thereby optimizing the use of polymeric

133 material.

134 **2. Materials and methods**

135 2.1 Octet lattice design

136 Two configurations of octet lattices were fabricated as reinforcements for the ultra-high-

137 performance concrete: one with a low volume reinforcement ratio (19.2%) and one with a high

138 volume reinforcement ratio (33.7%). The higher reinforcement of 33.7% was achieved by

139 increasing the member diameter of the octet unit cells, as shown in Figure 1. The member

140 diameters were chosen to ensure that they were several times greater than the extrusion nozzle

141 diameter of the 3D printer used (nozzle diameters were 1.2 mm for the flexural specimens and

142 0.4 mm for the compressive specimens), meaning that the octet geometry could be resolved

143 accurately and repeatably by the printer. The unit cell lengths of 11.7 and 23.5 mm were selected

144 to be large enough that the cement mix could flow easily through the interstices of the lattice,

145 and yet small enough that multiple unit cells could be incorporated into a sample that could be

146 printed in a reasonable time and whose size was manageable for testing. The member diameter

147 and unit cell lengths in turn determined the lattice volume fractions.
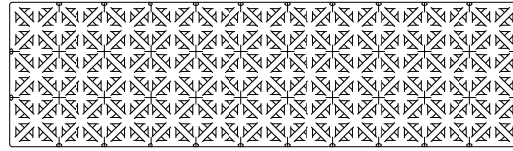
(a)
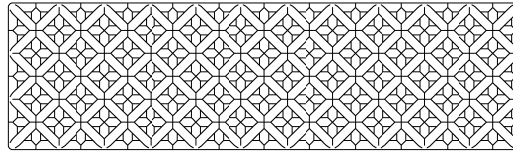
(b)

148
149 *Figure 1 – the two octet lattice designs. (a) 19.2% volume fraction and (b) 33.7% volume fraction. The lattice in (b) has thicker*
150 *members, and thus a higher volume fraction than (a).*

151   Cube and beam shaped lattices as shown in Figure 2 were 3D printed. These lattices were then

152   infiltrated with an ultra-high-performance concrete and tested in compression and four-point

153   bending, respectively. The specimens' dimensions were chosen so that there were at least three

154   unit cells in any direction, and are given in Table 1.
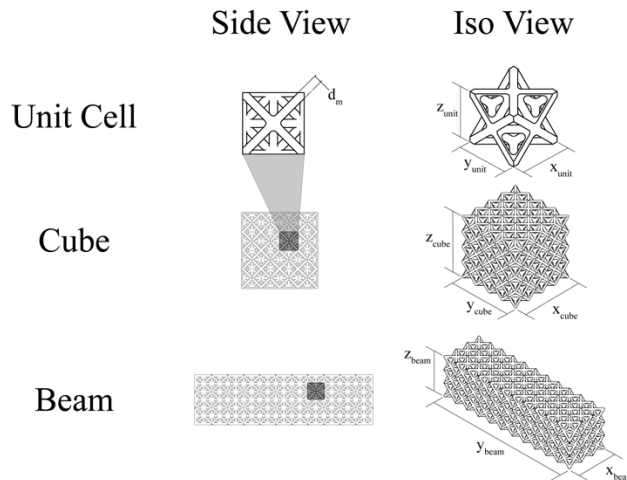
155
156 *Figure 2 - Cube and beam lattice specimen descriptions*

157 *Table 1 - Geometry description for compression cube and flexural beam specimens*

Specimen description	Member diameter, d_m (mm)	Lattice bounding dimensions (mm^3)	Lattice-reinforced concrete bounding dimensions (mm^3)	Number of lattice unit cells across	Unit cell length, x_{unit} (mm)

8

Compression cubes	19.2% design	1.6	48.5 × 48.5 × 48.5	50.8 × 50.8 × 50.8	4 × 4 × 4	11.7
	33.7% design	2.3	49.3 × 49.3 × 49.3			
Flexural beams	19.2% design	3.2	73.6 × 73.6 × 261.3	76.2 × 76.2 × 279.4	3 × 3 × 11	23.5
	33.7% design	4.6	74.9 × 74.9 × 262.8			

158 While the octet's volume percentages remained the same for compressive and flexural

159 specimens, the scale of the octet structure changed. The octets are doubled in scale for flexural

160 specimens compared to the compressive specimens; the octet member diameters and unit cell

161 lengths are listed in Table 1.
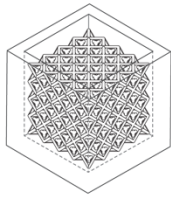
162 2.2 Fabrication

163 The lattice prisms for the flexure tests were 3D printed with PLA on a LulzBot TAZ 6 machine

164 using a 1.2 mm diameter nozzle, as shown in Figure 3a. The 1.2 mm diameter nozzle is rather

165 coarse, which allows each beam to be printed in less than 24 hours. The thermomechanical

166 properties of PLA allowed these lattices to be printed without any support structures. To

167 fabricate the compression cubes from PLA, a BCN3D Sigma with a 0.4 mm nozzle diameter was

168 used which also did not require any support material. The ABS cube lattices were produced

169 using a Stratasys Dimension 1200es with T16 model tip using Stratasys ABSPlus model material

170 and Stratasys P400SR support material. After printing, the support material was dissolved in an

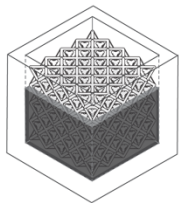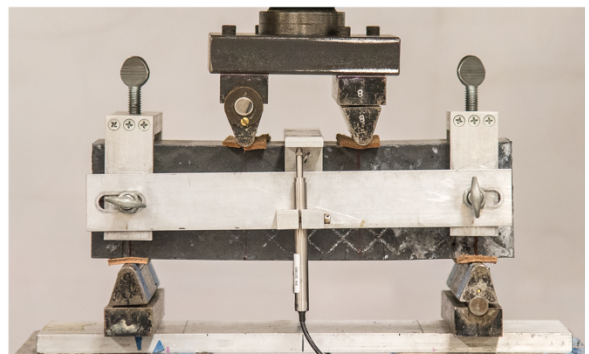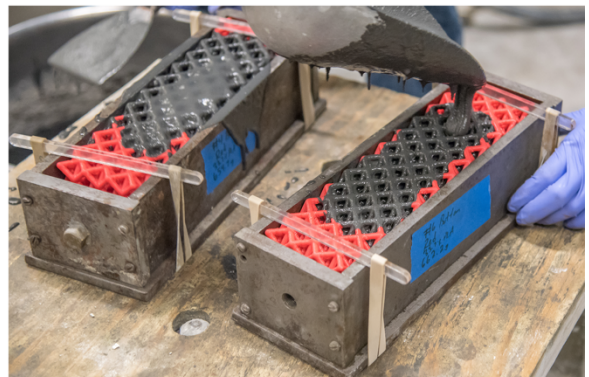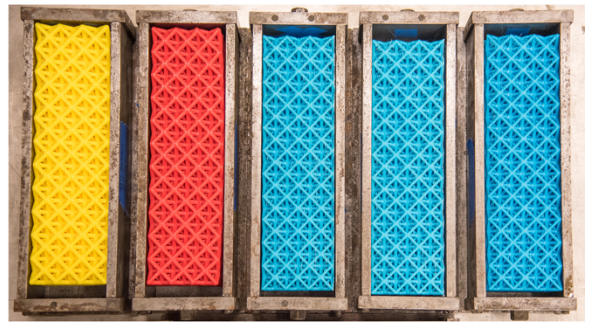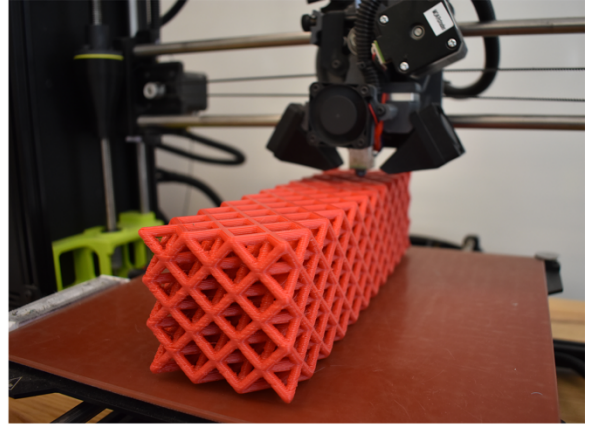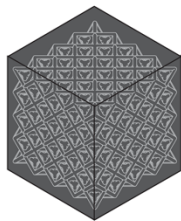171 ultrasonic bath of 2% concentration sodium hydroxide (Stratasys WaterWorks).

172

173

Figure 3 - Fabrication of lattice-reinforced concrete beams. (a) 3D printing of the polymeric lattice, (b) placement of lattices of
different reinforcing ratios inside molds, (c) infiltration of the lattices by an ultra-high-performance concrete, and (d) cured
beam ready to be tested.

177   Both cube and prism lattices were infiltrated with an ultra-high-performance concrete; the

178   UHPC's weight proportions are listed in Table 2. The 7-day compressive strength of a similar

179   UHPC is 119 MPa; further information on the UHPC mixture, development, and mechanical

180   properties may be found in [23–26]. To create lattice-reinforced concrete beams, the lattices

181   were placed into molds (Figure 3b), and the lattices' orientations were controlled so that the

182   flexural tests' loading direction was aligned with the printer's build direction. Having the tension

183   in the specimens aligned with the printed filaments ensures optimal mechanical properties. The

184   lattices were then infiltrated with UHPC (Figure 3c), and a vibration table was used to assist with

185   the infiltration. The addition of fly ash and superplasticizer resulted in a highly workable

186   concrete, which allowed each lattice to be fully infiltrated. The same procedure was followed to

187   cast lattice-reinforced concrete cubes.

188   The performance of the lattice-reinforced specimens is compared to a plain UHPC beam

189   and an ultra-high-performance fiber-reinforced concrete (UHPFRC) beam reinforced with 1.4%

190   PLA fibers (6 mm length, 1.3 denier per filament). Note that 1.4% by volume of fibers was the

191   highest volume percent that could be incorporated into the UHPC mix while still allowing the

192   mix to be workable enough to cast a rectangular beam.

193   All beams and cube specimens were stored and cured in a fog room (with 95% relative

194   humidity at room temperature) before testing on day 7.

195

196

197

198   *Table 2 - Weight proportions for the ultra-high-performance concrete mix*

Ingredient	Weight proportion
Cement	1.0
Fly ash	0.1
Water	0.26
Superplasticizer	0.02
Silica sand 1 (460 μm)	0.6
Silica sand 2 (120 μm)	0.3
Glass powder	0.25
Silica fume	0.25

199

200   2.3 Uniaxial compression and four-point flexural tests

201   Mechanical testing was carried out on a Universal Testing Machine with a 530 kN load cell. The

202   eight compression tests were performed according to ASTM C109 [28]. The nine beam

203   specimens were tested in four-point bending according to ASTM C1609 [29] with a 22.9 cm

204   span length. For both compression and flexural tests, the displacements were measured with two

205   linear variable differential transformers (LVDTs) — one at the front of the specimens, and one at

206   the back — and the measurements were averaged to compute the midspan deflection. On one of

207   the 19.2% lattice-reinforced beams, and one of the 33.7% lattice-reinforced beams, a digital

208   image correlation (DIC) technique was utilized instead of a second LVDT. For these two beams,

209   spackle patterns (black dots on a white background) were spray-painted onto the front side and a

210   Canon EOS 6D camera with a 100 mm macro lens then captured the displacement on the front

211   side. The midspan deflection was then determined by averaging the displacement measured with

212   DIC and the displacement measured with the LVDT.

213 **3. Results and discussion**

214 3.1 Uniaxial compression results

215 The lattice-reinforced UHPC's uniaxial compression results and the number of specimens tested

216 are given in Table 3. Both the PLA and ABS lattice-reinforced cubes exhibit a lower

217 compressive strength at the higher reinforcement percentage of 33.7% than at 19.2% polymer

218 volume fraction. While only one PLA specimen was tested for each reinforcing ratio, the results

219 suggest a common trend with the ABS results, whereby an increase in reinforcing ratio from

220 19.2% to 33.7% leads to a reduction in compressive strength. The smaller volume of UHPC at

221 33.7% lattice-reinforcement is responsible for the strength reduction since less of the high

222 compressive-modulus UHPC is being incorporated into these lattices. A large reduction in

223 strength was observed with the 33.7% ABS lattice-reinforced cubes. Both the 19.2% and 33.7%

224 ABS lattice-reinforced cubes show high strains at the peak stress, as well as high strain energy

225 densities. The 95% confidence intervals for the mean strain energy densities overlap for the

226 19.2% and 33.7% ABS-reinforced specimens.

227 *Table 3 - Description and results of uniaxial compression tests. Values indicate 95% confidence intervals of the mean.*

Cube description	Compressive strength (MPa)	Strain at peak stress (mm/mm)	Strain energy density (MPa)
19.2% PLA lattice-reinforcement (N = 1)	45.3	0.0114	1.86
33.7% PLA lattice-reinforcement (N = 1)	43.4	0.0161	2.09
19.2% ABS lattice-reinforcement (N = 3)	49.0 ± 1.0	0.0079 ± 0.0005	1.94 ± 0.13
33.7% ABS lattice-reinforcement (N = 3)	38.3 ± 6.0	0.0116 ± 0.0036	1.88 ± 0.32

228 N = number of specimens

229   Figure 4 shows the compressive stress–strain curves for the two types of reinforcement

230   ratios: three curves for the 19.2% ABS lattice-reinforced UHPC cubes, and three curves for the

231   33.7% ABS lattice-reinforced UHPC cubes.

232   The concrete cubes with the larger amount of reinforcement exhibit a larger variability in

233   stress–strain behavior, as shown by both Figure 4 and by the 95% confidence intervals for the

234   compressive strength shown in Table 3. The larger variability in the 33.7% lattices may be

235   caused by their smaller openings compared to the 19.2% lattices, which makes their infiltration

236   with UHPC more difficult and hence less uniform (due to possible air voids). On the other hand,

237   these composites exhibit smooth softening behavior up to high strain levels. In comparison,

238   UHPC (not shown here) does not exhibit softening behavior due to its high brittleness.
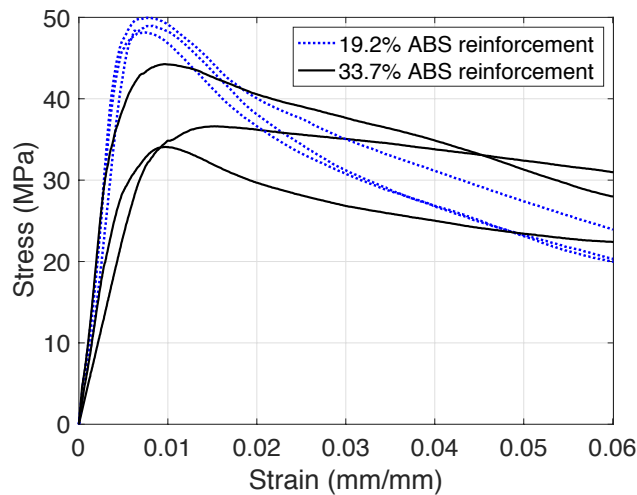
239

240   *Figure 4 - Compressive stress-strain curves for ABS lattice-reinforced UHPC with 19.2% reinforcement and 33.7%*
241   *reinforcement.*

242   The compressive stress-strain curves for both ABS and PLA lattice-reinforced UHPC at

243   19.2% and 33.7% reinforcement, respectively, are shown in Figure 5. At both reinforcement

244   ratios, the ABS and PLA lattice-reinforced samples perform similarly, as they exhibit similar

245   compressive strengths and strain energy densities. From these results, it appears that PLA-

246   reinforced UHPC may reach a higher strain at peak energy than ABS reinforced UHPC, but the

14

247   overall stress–strain curve characteristics are highly similar, and more tests need to be conducted

248   to form statistical conclusions. Figure 5 also shows the compressive behavior of the ABS lattices

249   (without UHPC), and while both the 19.2% and 33.7% ABS lattices exhibit high ductility, they

250   also exhibit low compressive strengths.
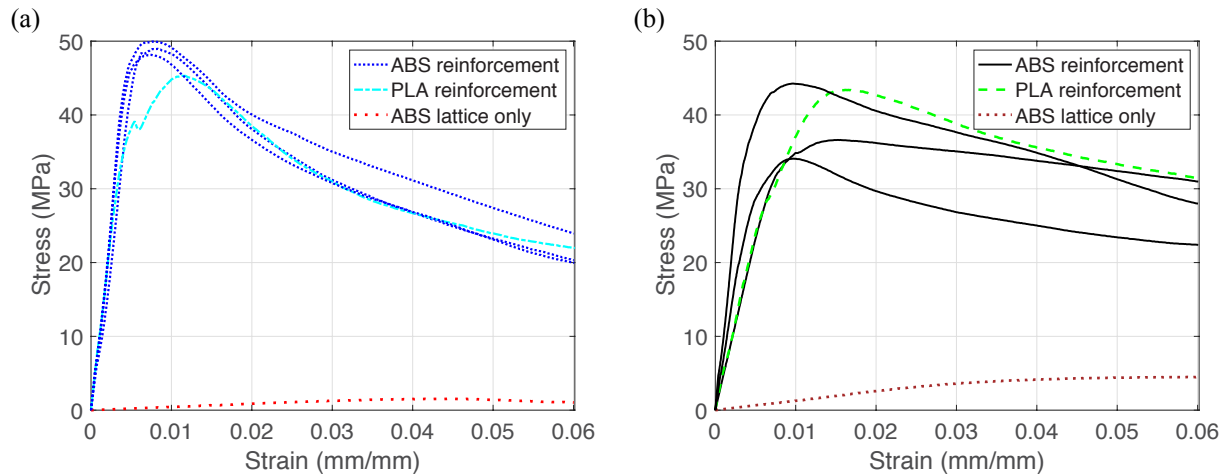
252 *Figure 5 - Compressive stress-strain curves. The response of the pure lattice and the UHPC reinforced with PLA and ABS*
253 *lattices is shown in (a) for 19.2% reinforcement and in (b) for 33.7% reinforcement.*

254 3.2 Four-point bending results

255   The flexural results of the PLA lattice-reinforced UHPC specimens are summarized in Table 4.

256   Note that all flexural specimens use PLA and not ABS, since PLA lattices do not require support

257   structures to print at this scale, but ABS lattices would require the extra steps to dissolve the

258   support material.

259   In these four-point bending tests, the 33.7% lattice-reinforced beams exhibit a higher

260   peak load than the 19.2% lattice-reinforced beams. Both the 19.2% and 33.7% lattice-reinforced

261   beams show high deflections at peak load and high toughness. The 95% confidence intervals for

262   the mean toughness overlap for the 19.2% and 33.7% reinforcement ratios.

15

263 *Table 4 – Four-point flexure results. Values indicate 95% confidence intervals of the mean.*

Beam description	Peak load (kN)	Deflection at peak (mm)	Toughness (kN·mm)*
19.2% PLA lattice-reinforcement (N = 3)	14.6 ± 0.4	1.8 ± 0.4	17.5 ± 0.5
33.7% PLA lattice-reinforcement (N = 4)	20.1 ± 4.3	2.4 ± 0.6	17.5 ± 0.9
UHPC only (N = 1)	13.0	0.027	0.20
1.4% PLA fiber-reinforcement (N = 1)	6.6	0.021	0.10

264 N = Number of specimens
265 * Toughness at 1.52 mm midpoint deflection

266 The load–midpoint deflection curves of the flexural beams are shown in Figure 6. For midpoint

267 deflections up to 1.52 mm (*i.e.* the span length divided by 150, as specified by [28]), all

268 specimens behave similarly, independent of their reinforcing ratios (Figure 6a). The behavior

269 differs at larger deflections, where the beams with a higher reinforcement ratio achieve higher

270 loads (as shown in Figure 6b), which is opposite to the compression results. This difference in

271 behavior at higher deflections is due to the increased crack growth resistance that a larger

272 reinforcement ratio provides.

273 Similar to the compression results the beams with the higher reinforcement ratio exhibit a

274 larger variability in their load–deflection curves due to the small openings of the 33.7% lattices

275 that make the infiltration of UHPC less uniform. Figure 6b shows one 33.7% lattice-reinforced

276 beam which underperforms compared to the other three samples; however, since its net

277 deflection at peak load is not more than 1.5 interquartile ranges below the first quartile and it is

278 not more than 1.5 interquartile ranges above the third quartile, we do not classify it as an outlier.

279 While all lattice-reinforced beams reveal high ductility, the beam reinforced with

280 1.4 vol% PLA fibers shown in Figure 6 by the red line exhibits very brittle behavior up to failure.

281   Hence, the highest volume fraction of fibers that could be incorporated into the UHPC mixture

282   while maintaining a workable mix was not sufficient to provide any crack growth resistance.

283   While the volume fractions of polymer fibers and printed reinforcement used in this work are

284   very different (1.4 vol% fibers *vs* 19.2–33.7 vol% lattices), the results shown for PVA fiber

285   reinforcement represent the best practically achievable option with this particular reinforcement

286   approach and mortar composition.

287   The brittle performance of the plain UHPC beam agrees with the mechanical properties

288   of a similar UHPC tested in [26]. In comparison to the unreinforced, UHPC-only beam, the

289   lattice-reinforced beams are able to achieve higher flexural loads, since the reinforcement

290   prevents a dominant crack from propagating through the beam.
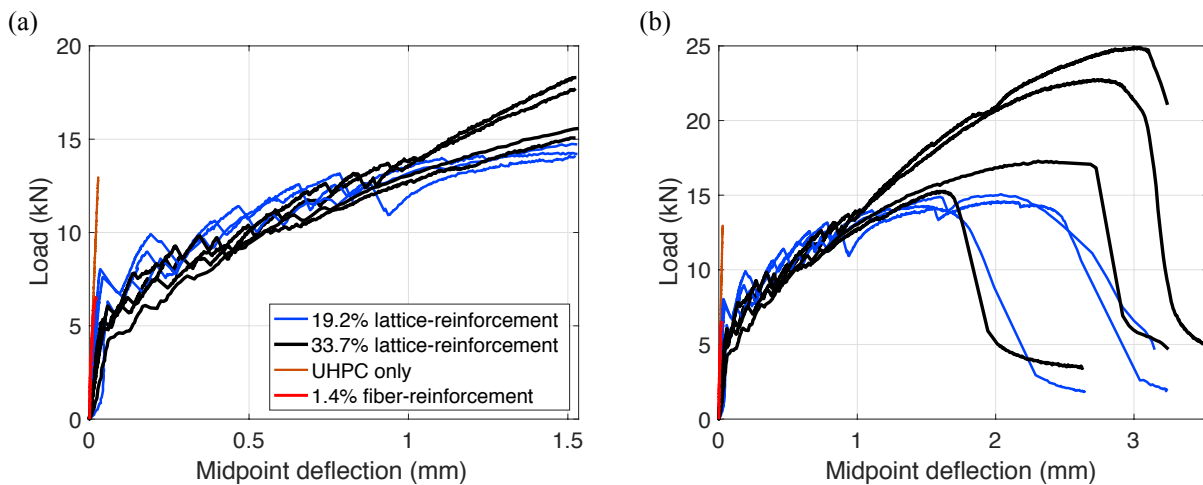
291

292 *Figure 6 – Load–deflection curves for flexural specimens with varying amounts of polymeric reinforcement. The loading curve is*
293 *plotted (a) until a maximum deflection of 1.52 mm (which was used for the toughness calculations in Table 4) and (b) until*
294 *failure of the beams.*

295

296   3.3 Failure characteristics

297   DIC software (OpteCAL) was utilized to investigate the sequence of crack initiation and crack

298   pattern of a 19.2% lattice-reinforced beam during four-point bending. Figure 7 shows the strain

17

299 field across the front face of the specimen. The strain field is then correlated with the load-

300 deflection curve.
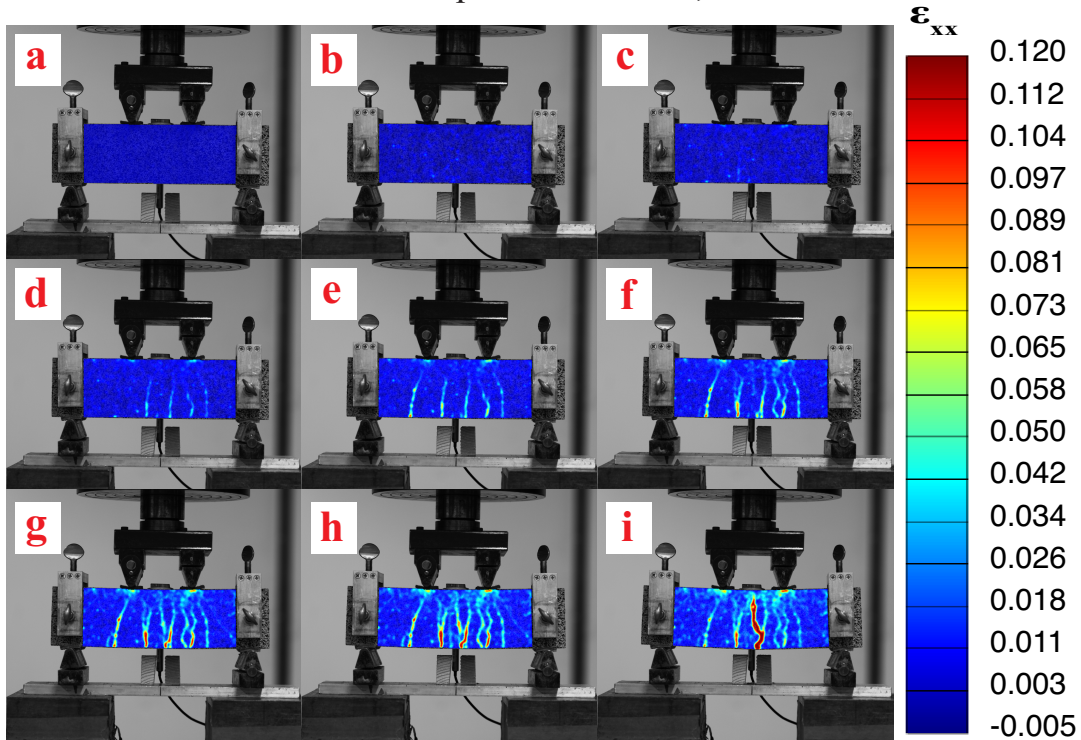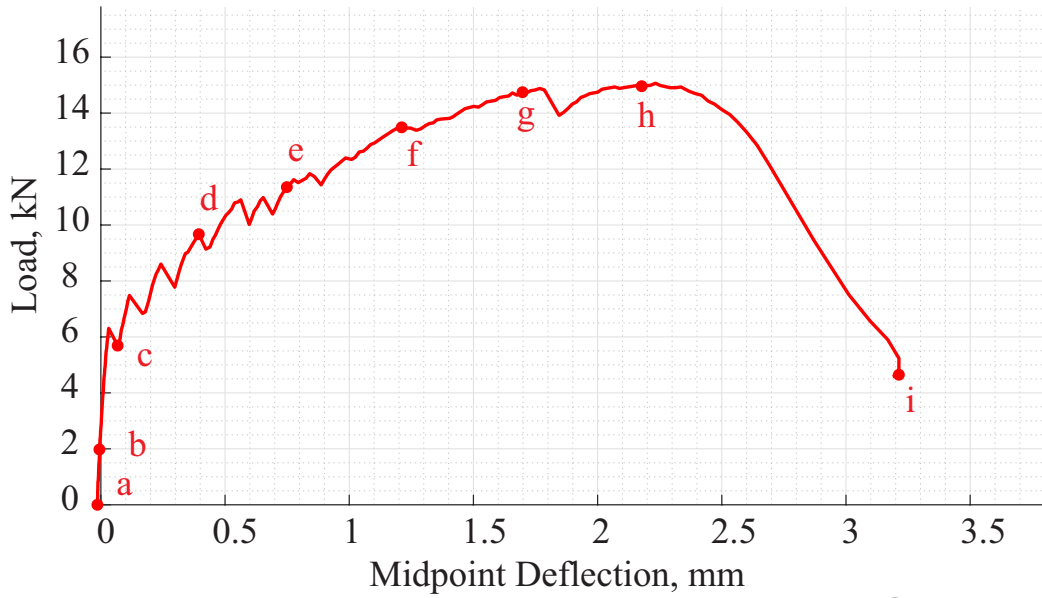
301

302 *Figure 7 - Strain field across the front surface of flexural beams as measured with digital image correlation techniques. The*
303 *progression of cracks is shown at various points across the load-deflection curve for the 19.2% lattice-reinforcement beam.*

304   From (a) to (b), while the beam is in its elastic regime, no cracking could be observed.

305   Hairline cracks initiate between (b) and (c), followed by multiple crack formation at (d). The

306   multiple cracks increase in width from (d) to (f) in the tension zone while propagating towards

307   the compression zone. Each of the multiple cracks continue to carry load, bifurcate and further

308   increase in width between (g) and (h), which causes a flattening of the load–deflection curve.

309   Eventually one of the multiple cracks becomes the dominant crack which leads to a drastic

310   reduction in load capacity of the beam. The strain field of the specimen just prior to failure is

311   shown in (i), with the dominant crack visible in red. DIC analysis for a 33.7% lattice-reinforced

312   beam (not shown here) shows failure mechanism trends that are identical to the mechanisms

313   exhibited by this 19.2% lattice-reinforced beam, with the 33.7% lattice-reinforced beam

314   exhibiting a higher ultimate load.

315   Figure 8 contains images of representative fracture surfaces and side views of a 19.7%

316   lattice-reinforced beam (Figure 8a, b), a 33.7% lattice-reinforced beam (Figure 8c, d), and the

317   1.4% fiber-reinforced beam (Figure 8e, f). Both lattice-reinforced beams reveal rough fracture

318   surfaces which indicates that the cracks traveled through a tortuous path. This type of cracking

319   contributes to the high ductility observed in these lattice-reinforced beams. The images of the

320   lattice-reinforced beams also show step marks in the concrete, which are locations where the

321   concrete debonded from the polymeric lattice, leading to high strain energy density values. The

322   polymeric members show stress-whitening, indicating that they carried tensile stresses.

323   Furthermore, the polymeric members' cup-and-cone fracture surfaces suggest that the fracture

324   was ductile.

325   By contrast, the fiber-reinforced beams show smooth fracture surfaces, with no detectable

326   fiber pull-out. This type of fracture surface is indicative of either a lack of debonding between

19

327   the fibers and the matrix or inhomogeneous fiber distribution due to the low workability of the

328   mix. Lattice-reinforcement has the advantage that it allows us to control precisely the distribution

329   of the reinforcement within a structure.

330   Whereas in Salazar et al. [18], the polymeric lattice of the lattice-reinforced mortar

331   samples fractured uniformly along a plane, the lattice-reinforced UHPC shown here does not

332   have the polymeric members fracture along a single plane. The difference is due to the print

333   direction, as previous research has shown that aligning the printed layers to be perpendicular to

334   the crack plane results in increased tensile strength and fracture toughness [30,31]. The current

335   work has the lattices printed in such a way that the build direction is aligned with the loading

336   direction, as opposed to having the build and loading directions be orthogonal as in [18], which

337   allowed the crack to cleave in-between printed layers.

338

339
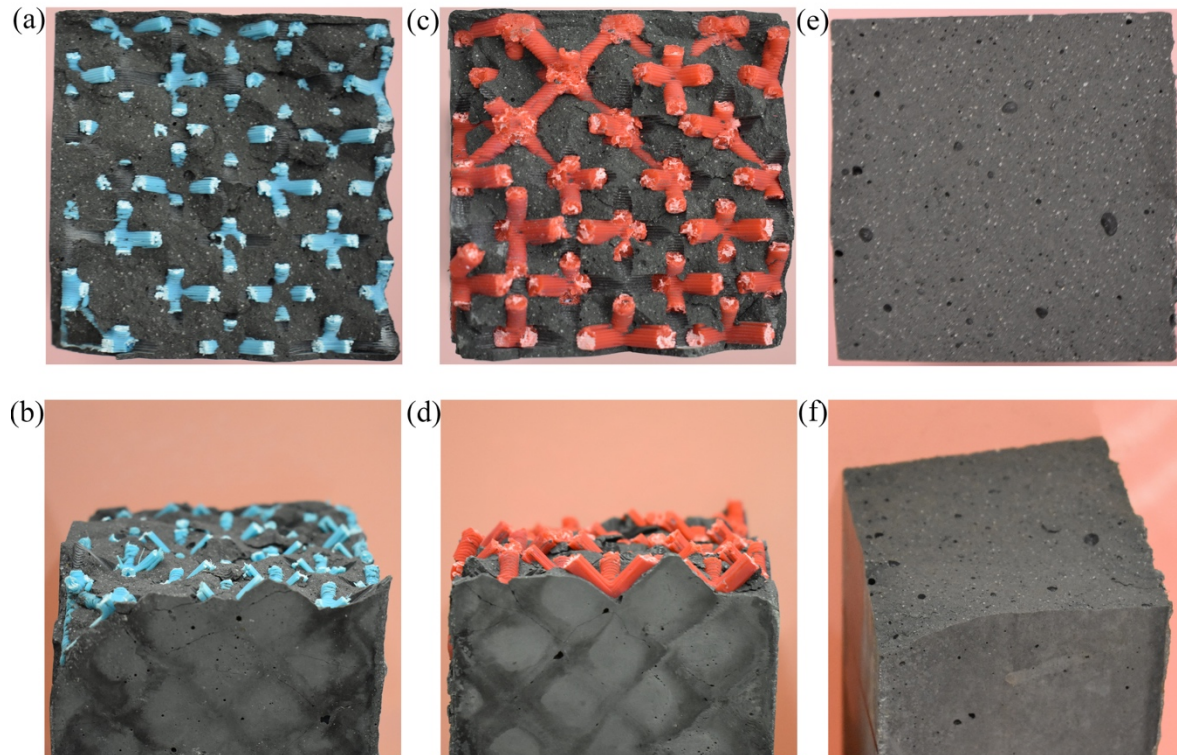
Figure 8 - Direct and side views of fracture surfaces of flexure specimens. (a) and (b) are representative of the 19.7% lattice-reinforced beams; (c) and (d) represent the 33.7% lattice-reinforced beams; (e) and (f) are the fiber-reinforced beam. Note that the dominant crack did not propagate through the entire beam, and beams were opened manually post-testing.

4. Conclusion

Lattice-reinforced concrete samples were created by fabricating polymeric lattices and infiltrating these lattices with ultra-high-performance concrete. These lattice-reinforced concrete samples exhibited high ductility in both compression and flexure. Compressive tests showed high strain density values, with the polymeric material choice (PLA or ABS) not having a significant effect. Increasing the percentage of the lattice reinforcement, however, led to a decrease and a higher variability in their compressive strength. Regarding flexure, all lattice-reinforced beams exhibited strain hardening up to peak load and the highest peak loads were observed with the higher lattice reinforcement of 33.7%. DIC was utilized to investigate the strain fields and to obtain information on the crack pattern during flexural loading. The results

21

353 revealed multiple cracking and crack widening in these octet lattice-reinforced beams up to peak

354 load.

355   While this paper focused on 3D-printed PLA and ABS octet lattice-reinforced structures

356 as proofs of concept, the method itself is not limited to this specific kind of lattice geometry or to

357 these particular polymeric materials. The ideal reinforcement geometry and material will depend

358 on the application. Lattice reinforcement allows the placement of the reinforcement material to

359 be controlled and hence optimized for specific loading scenarios — for example by increasing

360 the volume fraction of reinforcement material in regions of higher expected tensile stress.

361 Moreover, the optimal choice of polymeric material is a matter for future study, and the long-

362 term stability of candidate polymers in contact with cementitious materials will need to be tested.

363   Fused deposition modeling 3D printing is known to be an anisotropic process, with 3D-

364 printed components being stronger when loaded along extruded polymer filaments, and weaker

365 when loaded across the interfaces between adjacent filaments. In this paper the specimens were

366 printed such that the build direction was aligned with the flexural tests' loading direction.

367 Therefore, the tension in the samples was predominantly aligned with the printed filaments. In

368 this case, the cracks are forced to propagate through multiple printed layers, and not solely

369 between layers. This approach allowed our specimens to reach as high a toughness as possible

370 for the chosen manufacturing process.

371   The choice of 3D printing for lattice fabrication enabled rapid prototyping. Fabrication at

372 larger scales and volumes — such as for building construction — could be accomplished by

373 robotic extrusion printing with larger nozzles; the higher material deposition rates would

374 substantially reduce production times. Indeed, the use of large-scale robotic extrusion printers in

22

375   which individual extruded filaments of polymer are typically 5–10 mm in diameter would not

376   only increase throughput but would also eliminate layering effects within the members of the

377   printed lattices, since a single large extruded filament could serve as a complete member. If the

378   member and unit cell sizes of these lattices were to be increased to aid high-volume production,

379   while the materials remained similar, it can be anticipated that the basic failure mechanism

380   would remain the same, although this would need to be confirmed through further experiments.

381   It may also be possible to develop injection-molding processes for geometrically regular

382   reinforcement lattices. The octet lattice geometry is defined by approximately triangular,

383   intersecting prismatic voids, so in principle a mold could be engineered with multiple retractable,

384   interlocking cores to create the 3D lattice. While the development costs of such an approach

385   would probably be very considerable, they may be warranted by the increased production rate.

386   Layering and directional effects could also be minimized by molding rather than printing.

396   **Data Availability**

397 The raw data required to reproduce these findings are available to download from

398 http://dx.doi.org/10.17632/wv7hvgg8c7.1

399 **References**

400 [1]   Bolander JE, Choi S. Fracture of fiber-reinforced cement composites : effects of fiber

401   dispersion 2008:73–86. https://doi.org/10.1007/s10704-008-9269-4.

402 [2]   Stähli P, Custer R, Van Mier JGM. On flow properties, fibre distribution, fibre orientation

403   and flexural behaviour of FRC. Mater Struct Constr 2008;41:189–96.

404   https://doi.org/10.1617/s11527-007-9229-x.

405 [3]   Abrishambaf A, Barros JAO, Cunha VMCF. Relation between fibre distribution and post-

406   cracking behaviour in steel fibre reinforced self-compacting concrete panels. Cem Concr

407   Res 2013;51:57–66. https://doi.org/10.1016/j.cemconres.2013.04.009.

408 [4]   Sarmiento E V., Geiker MR, Kanstad T. Influence of fibre distribution and orientation on

409   the flexural behaviour of beams cast from flowable hybrid polymer-steel FRC. Constr

410   Build Mater 2016;109:166–76. https://doi.org/10.1016/j.conbuildmat.2016.02.005.

411 [5]   Zhou B, Uchida Y. Relationship between fiber orientation/distribution and post-cracking

412   behaviour in ultra-high-performance fiber-reinforced concrete (UHPFRC). Cem Concr

413   Compos 2017;83:66–75. https://doi.org/10.1016/j.cemconcomp.2017.07.007.

414 [6]   Stähli P, van Mier JGM. Manufacturing, fibre anisotropy and fracture of hybrid fibre

415   concrete. Eng Fract Mech 2007;74:223–42.

416   https://doi.org/10.1016/j.engfracmech.2006.01.028.

417 [7]   Švec O, Žirgulis G, Bolander JE, Stang H. Influence of formwork surface on the

418   orientation of steel fibres within self-compacting concrete and on the mechanical

419   properties of cast structural elements. Cem Concr Compos 2014;50:60–72.

420   https://doi.org/10.1016/j.cemconcomp.2013.12.002.

421 [8] Hegger J, Will N, Bruckermann O, Voss S. Load-bearing behaviour and simulation of

422   textile reinforced concrete. Mater Struct Constr 2006;39:765–76.

423   https://doi.org/10.1617/s11527-005-9039-y.

424 [9] Hegger J, Will N, Rüberg K. Textile reinforced concrete-A new composite material. Adv

425   Constr Mater 2007 2007:147–56.

426 [10] Brückner A, Ortlepp R, Curbach M. Textile reinforced concrete for strengthening in

427   bending and shear. Mater Struct Constr 2006;39:741–8. https://doi.org/10.1617/s11527-

428   005-9027-2.

429 [11] Hegger J, Voss S. Investigations on the bearing behaviour and application potential of

430   textile reinforced concrete 2008;30:2050–6.

431   https://doi.org/10.1016/j.engstruct.2008.01.006.

432 [12] Schladitz F, Frenzel M, Ehlig D, Curbach M. Bending load capacity of reinforced

433   concrete slabs strengthened with textile reinforced concrete. Eng Struct 2012;40:317–26.

434   https://doi.org/10.1016/j.engstruct.2012.02.029.

435 [13] Vervloet J, Van Itterbeeck P, Verbruggen S, El Kadi M, De Munck M, Wastiels J, et al.

436   Experimental investigation of the buckling behaviour of Textile Reinforced Cement

437   sandwich panels with varying face thickness using Digital Image Correlation. Constr

438   Build Mater 2019;194:24–31. https://doi.org/10.1016/j.conbuildmat.2018.11.015.

25

439 [14] Colombo IG, Colombo M, Prisco M. Bending behaviour of Textile Reinforced Concrete

440   sandwich beams. Constr Build Mater 2015;95:675–85.

441   https://doi.org/10.1016/j.conbuildmat.2015.07.169.

442 [15] Williams Portal N, Flansbjer M, Zandi K, Wlasak L, Malaga K. Bending behaviour of

443   novel Textile Reinforced Concrete-foamed concrete (TRC-FC) sandwich elements.

444   Compos Struct 2017;177:104–18. https://doi.org/10.1016/j.compstruct.2017.06.051.

445 [16] Deshpande VS, Fleck NA, Ashby MF. Effective properties of the octet-truss lattice

446   material. J Mech Phys Solids 2001;49:1747–69. https://doi.org/10.1016/S0022-

447   5096(01)00010-2.

448 [17] O'Masta MR, Dong L, St-Pierre L, Wadley HNG, Deshpande VS. The fracture toughness

449   of octet-truss lattices. J Mech Phys Solids 2017;98:271–89.

450   https://doi.org/10.1016/j.jmps.2016.09.009.

451 [18] Salazar B, Williams I, Aghdasi P, Ostertag C, Taylor H. International Congress on

452   Polymers in Concrete (ICPIC 2018). Int Congr Polym Concr (ICPIC 2018) 2018:261–6.

453   https://doi.org/10.1007/978-3-319-78175-4.

454 [19] Farina I, Fabbrocino F, Carpentieri G, Modano M, Amendola A, Goodall R, et al. On the

455   reinforcement of cement mortars through 3D printed polymeric and metallic fibers.

456   Compos Part B Eng 2016;90:76–85. https://doi.org/10.1016/j.compositesb.2015.12.006.

457 [20] Nam YJ, Hwang YK, Park JW, Lim YM. Feasibility study to control fiber distribution for

458   enhancement of composite properties via three-dimensional printing. Mech Adv Mater

459   Struct 2019;26:465–9. https://doi.org/10.1080/15376494.2018.1432809.

460 [21] Rosewitz JA, Choshali HA, Rahbar N. Bioinspired design of architected cement-polymer

461 composites. Cem Concr Compos 2019;96:252–65.

462 https://doi.org/10.1016/j.cemconcomp.2018.12.010.

463 [22] Xu Y, Šavija B. Development of strain hardening cementitious composite (SHCC)

464 reinforced with 3D printed polymeric reinforcement: Mechanical properties. Compos Part

465 B Eng 2019;174. https://doi.org/10.1016/j.compositesb.2019.107011.

466 [23] Aghdasi P. Development and Characterization of Green Ultra-High Performance Fiber-

467 Reinforced Concrete (G-UHP-FRC) for Structural and Non-Structural Applications.

468 University of California, Berkeley, 2019.

469 [24] Aghdasi P, Heid AE, Chao SH. Developing ultra-high-performance fiber-reinforced

470 concrete for large-scale structural applications. ACI Mater J 2016;113:559–69.

471 https://doi.org/10.14359/51689103.

472 [25] Aghdasi P, Ostertag CP. Green ultra-high performance fiber-reinforced concrete (G-UHP-

473 FRC). Constr Build Mater 2018;190:246–54.

474 https://doi.org/10.1016/j.conbuildmat.2018.09.111.

475 [26] Aghdasi P, Williams ID, Salazar B, Panditi N, Taylor HK, Ostertag CP. An Octet-Truss

476 Engineered Concrete (OTEC) for lightweight structures. Compos Struct 2019;207:373–

477 84. https://doi.org/10.1016/j.compstruct.2018.09.011.

478 [27] Branch Technology n.d. https://www.branch.technology (accessed July 17, 2020).

479 [28] ASTM C109/C109M-16a. Standard Test Method for Compressive Strength of Hydraulic

480 Cement Mortars (Using 2-in. or [50-mm] Cube Specimens). ASTM Int 2016.

481 https://doi.org/10.1520/C0109.

482 [29] ASTM C1609/C1609M-19. Standard Test Method for Flexural Performance of Fiber-

483 Reinforced Concrete (Using Beam With Third-Point Loading). ASTM Int 2005.

484 https://doi.org/10.1520/C1609.

485 [30] Zou R, Xia Y, Liu S, Hu P, Hou W, Hu Q, et al. Isotropic and anisotropic elasticity and

486 yielding of 3D printed material. Compos Part B Eng 2016;99:506–13.

487 https://doi.org/10.1016/j.compositesb.2016.06.009.

488 [31] McLouth TD, Severino J V., Adams PM, Patel DN, Zaldivar RJ. The impact of print

489 orientation and raster pattern on fracture toughness in additively manufactured ABS.

490 Addit Manuf 2017;18:103–9. https://doi.org/10.1016/j.addma.2017.09.003.

491